MODELING STIMULUS-FREQUENCY OTOACOUSTIC EMISSIONS IN THE GECKO

Christopher Bergevin [1] and Christopher A. Shera [2,3]

[1]Department of Mathematics, University of Arizona; [2]Eaton-Peabody Laboratory, Massachusetts Eye & Ear Infirmary [3]Department of Otology & Laryngology, Harvard Medical School

MOTIVATION

- Stimulus-frequency otoacoustic emissions (SFOAEs) demonstrate significant phase-gradient delays on the order of a millisecond or longer in a wide array of species [Bergevin et al. 2008].

- Phase-gradient delays, defined as the slope of the emission phase with respect to stimulus frequency, are similar to delays measured in the time domain in both mammals and non-mammals [Schoonhoven et al. 2001; Withnell et al. 2005; Meenderink and Narins, 2005; Sisto et al. 2007].

- These delays are not due to the middle ear, whose contribution is on the order of tens of microseconds [Rosowski et al. 1985].

- It is not readily apparent where these delays arise from, particularly in species that lack a propagating traveling wave along the basilar membrane (BM).

QUESTION: *What is the mechanism that gives rise to significant delays observed in OAEs?*

BACKGROUND

- To address this question, we develop a model for a relatively simple ear where delays are significant (~1 ms) and BM traveling waves are not present, the idea being that 'travel time' is minimized as a confounding factor.

- We focus here on the inner ear of the gecko, a lizard that exhibits low thresholds and robust emissions. There is also a significant body of literature on various aspects of gecko auditory anatomy and physiology (e.g. auditory nerve fiber responses).

- The gecko inner ear consists of ~1000 hair cells sitting atop the relatively rigid basilar papilla, with regions of both a continuous and discretized overlying tectorial membrane coupling nearby cells together [Wever, 1978]

⟶ The general approach taken here is to model the ear as a series of (passive, linear) coupled oscillators

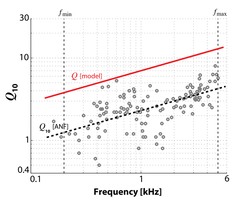

FIGURE 1 Tokay gecko auditory nerve fiber Q_{10} values near threshold [Manley et al. 1999]. The same study also traced the fibers back to the papilla, thereby providing a tonotopic map (and thus a space constant ℓ). These data were used to determine the model's free parameters. The red solid line shows model Q, where we use the approximation $Q = 3Q_{10}$.

MODEL

Assumptions
- middle ear delay is negligible
- inner fluids are incompressible and the pressure is uniform within each scalae
- papilla moves transversely as a rigid body (rotational modes are ignored)
- consider hair cells grouped together via a sallet, each as a resonant element (referred to as a *bundle* from here on out) [Aranyosi and Freeman, 2004]
- bundles are coupled only by motion of papilla (fluid coupling ignored)
- papilla is driven by a sinusoidal force (at angular frequency ω)
- system is linear and passive
- small degree of irregularity is manifest in tuning along papilla length

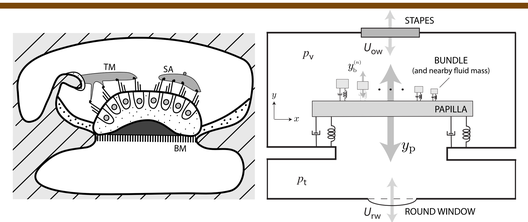

FIGURE 2 *Left:* Simplified transverse-radial cross-sectional schematic of the gecko inner-ear anatomy showing hair cells embedded in the papilla. Papilla has an effective area A_p and length $L = 0.1$ cm. The gecko is one of many lizard species that has sallets, discretized sections of tectorium that are thought to behave as resonant filters. White regions are fluid-filled, gray region represent the overlying tectorium, gray striped areas represent bone, and stippled areas are supporting cellular structures. Abbreviations: BM - basilar membrane, TM - tectorial membrane, SA - sallet. *Right:* Longitudinal-transverse cross-section of the model, consisting of a collection of linear oscillators coupled by the motion of the basilar papilla.

Equations of Motion

Papilla $m_p\ddot{y}_p = -k_p y_p - r_p\dot{y}_p + \sum_n k_b^{(n)}(y_b^{(n)} - y_p) + A_p(p_v - p_t)$

Bundle (n'th bundle along papilla length) $\ddot{y}_b^{(n)} = -\omega_b^{(n)2}\left[y_b^{(n)} - y_p\right] - \gamma_b^{(n)}\dot{y}_b^{(n)}$

time domain ⟷ frequency domain: $y(t) = \mathbf{Y}(\omega)e^{i\omega t}$

Papilla: $\mathbf{Y}_p\left[-\omega^2 m_p + i\omega r_p + k_p + \sum_n k_n\right] = \sum_n k_n \mathbf{Y}_n + A_p(\mathbf{P}_v - \mathbf{P}_t)$ Bundle: $\mathbf{Y}_n = \mathbf{Y}_p \frac{1}{1 - {\beta_n}^2 + i\beta_n/Q_n}$

Change of Variables

$y_b^{(n)} = y(x_n) = y_n$ *bundle longitudinal location (and similar notation for other parameters)*

$\omega_n = \sqrt{\frac{k_n}{m_n}} = \omega_{max}e^{-x_n/\ell}$ *n'th bundle characteristic frequency (CF)*

$\beta_n = \omega/\omega_n$ *ratio of bundle resonant and stimulus frequencies*

$Q_n = \omega_n/\gamma_n$ *bundle bandwidth*

$A_p(\mathbf{P}_v - \mathbf{P}_t)$ *pressure difference across papilla is driving stimulus*

An Emission Defined

$\mathbf{Y}_p\left[-\omega^2 m_p + i\omega r_p + k_p + \sum_n k_n \frac{-\beta_n^2 + i\beta_n/Q_n}{1 - \beta_n^2 + i\beta_n/Q_n}\right] = A_p(\mathbf{P}_v - \mathbf{P}_t)$ *combine both eqns. of motion in frequency domain*

Input Impedance

$i\omega\mathbf{Y}_p A_p = \mathbf{U}_{ow}$ *conservation of mass* ⟶ $\mathbf{Z} \equiv \frac{\mathbf{P}_v - \mathbf{P}_t}{\mathbf{U}_{ow}} = \frac{1}{i\omega A_p^2}\left[Z_p + \sum_n k_n \frac{-\beta_n^2 + i\beta_n/Q_n}{1 - \beta_n^2 + i\beta_n/Q_n}\right]$

Irregularity

$\tilde{Q}_n = Q_n(1 + \epsilon_n)$ ⟶ $\Delta\mathbf{Z} = \tilde{\mathbf{Z}} - \mathbf{Z}$ ⟶ $\boxed{\Delta\mathbf{P} \equiv \Delta\mathbf{Z}\,\mathbf{U}_{ow}}$

ϵ_n *is a small perturbation term*; *impedance difference between irregular and smooth conditions*; *papilla contributions cancel out*

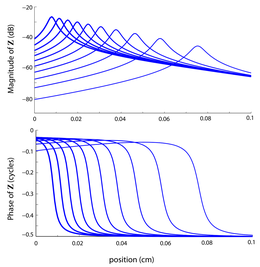

FIGURE 3 Model impedance ($\mathbf{Z}$) for ten different stimulus frequencies (thicker lines for higher driving frequency). The plot shows contributions from the bundles, papilla terms are neglected. [150 bundles with CFs from 0.2-5 kHz; 10 stimulus frequencies linearly spaced from 0.6-4 kHz]. Bundle stiffness (k_n) was assumed to vary exponentially.

Analytic Approximation

- To derive an approximate expression for the model phase-gradient delay, we make several simplifying assumptions (e.g., convert sum to integral, assuming bundle stiffness term is approximately constant, etc.).

- We validated the approximations using numerical analysis

$\Delta P \approx \frac{U_{ow}k_o\ell}{\omega A^2}\int_{\beta_0}^{\beta_L}\epsilon(x)\frac{A^2}{Q}e^{2i\theta}d\beta$ *rewrite expression for emission in continuous limit with suitable change of variables*

$\beta_L \equiv \omega/\omega_{min}$; $\beta_0 \equiv \omega/\omega_{max}$; $x = \ell\ln\left(\frac{\beta}{\beta_0}\right)$; $\frac{1}{1 - \beta^2 + i\beta/Q} \equiv A(\beta)e^{i\theta(\beta)}$ *transfer function for the harmonic oscillator*

express irregularity as composed of distinct spatial frequencies along length of papilla $\epsilon(x) = \sum_\kappa \epsilon_\kappa e^{i\kappa x}$ *given the strongly peaked nature of the integrand (Fig. 3) and by analogy to coherent reflection theory, we expect that only spatial frequencies close to some optimal value will contribute*

frequency dependence of emission phase (ϕ) comes primarily from this term, requiring us to determine κ_{opt}; the amplitude is a sharply peaked function (Fig.3), indicating the value of the integral is relatively constant with respect to stimulus frequency (ω)

⟶ $\Delta P \approx \frac{U_{ow}k_o\ell\epsilon_{\kappa_{opt}}}{\omega A^2}e^{-i\kappa_{opt}\ell\ln\beta_0}\int_{\beta_0}^{\beta_L}\frac{A^2(\beta)}{Q(\beta)}e^{i[\kappa_{opt}\ell\ln\beta + 2\theta(\beta)]}d\beta$

for the integral to be maximal, we require the phase be stationary about the magnitude peak (i.e., $\beta = 1$), allowing us to solve for the optimal spatial frequency $\frac{\partial}{\partial\beta}\left[\kappa_{opt}\ell\ln\beta + 2\theta(\beta)\right]|_{\beta=1} = 0$ ⟶ $\kappa_{opt} = -\frac{2}{\ell}\left.\frac{\partial\theta}{\partial\beta}\right|_{\beta=1} = -\frac{2\omega}{\ell}\frac{\partial\theta}{\partial\omega}$

in can be shown that for the harmonic oscillator $\left.\frac{\partial\theta}{\partial\omega}\right|_{\omega_o} = -\frac{Q}{f\pi}$ *from above, our expression for the model phase-gradient delay will be* $N_{OAE} = \frac{\kappa_{opt}\ell}{2\pi}$ *combining all our expressions we finally have....*

$\boxed{N_{OAE} \approx \frac{2Q}{\pi}}$ *thus, the phase gradient delay is directly proportional to the sharpness of tuning*

Phase-Gradient Delay

$\tau_{OAE} = -\frac{1}{2\pi}\frac{\partial\phi}{\partial f}$ where $\phi = \arg(\Delta P)$ ⟶ $\boxed{N_{OAE} = f\tau_{OAE}}$

MODEL RESULTS

- Impedance ($\mathbf{Z}$) shows a strongly peaked magnitude response and sharp phase transition centered about the bundle location with CF close to that of the driving frequency [Fig. 3].

- Model emission behavior ($\Delta\mathbf{P}$) shows magnitude peaks and valleys whose location depends on the underlying irregularity (random spatial noise). Significant phase accumulation is apparent [Fig. 4].

- The qualitative features observed in Fig. 4 are relatively insensitive to parameters such as the bundle stiffness k_n, total number of bundles (greater than ~20) or constants such as the papillar area A_p.

- Figure 5 shows that while variability is present, the mean phase-gradient delay (expressed in number of stimulus periods N) shows good correlation with the analytic approximation. Changes in the assumed Q produced corresponding changes in N. These results indicate that the emission phase-gradient delay (N) is directly proportional to the sharpness of tuning (Q).

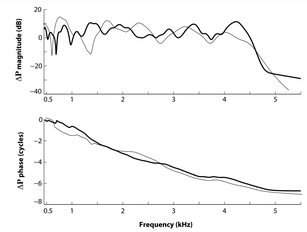

FIGURE 4 Model SFOAE results (magnitude and phase of $\Delta\mathbf{P}$). [150 bundles with CFs logarithmically distributed from 0.2 to 4.5 kHz]. ϵ_n was sampled from a Gaussian distribution with zero mean and a standard deviation of 0.03. Model results are shown for two different `ears' (i.e., different irregularity patterns).

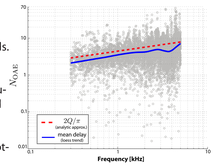

FIGURE 5 Model SFOAE phase-gradient delays expressed in stimulus periods. The solid curve is a trend line computed from the results for 20 different simulated ears (grey circles) and trend line (solid blue line). Analytic approximation (dashed red line) is also plotted.

COMPARISON TO OAE DATA

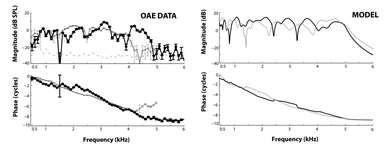

FIGURE 6 *Left:* Representative SFOAE data using a 20 dB SPL probe level in two geckos. The dashed line indicates the noise floor. *Right:* Model values of $\Delta\mathbf{P}$. The model papilla comprised 150 bundles with CFs logarithmically distributed from 0.2 to 5 kHz. A roughness factor of 3% was used. Model results are shown for two different `ears' to demonstrate the variability in features such as notch locations and phase slopes. The overall model magnitude was scaled to approximate those of the measurements.

- As shown in Fig. 6, the model captures many of the qualitative features of the OAE data: the magnitude roll-off outside the frequency range of ANF CFs, the spectral peaks and valleys unique to a given 'ear', and substantial phase accumulation.

- When the model Q values are chosen to match ANF responses, the model predicts generally realistic OAE delays (Fig.7)

- Below ~1 kHz, the predicted delays are longer than those measured. This low-frequency deviation is similar to that observed in mammals between measures of Q and N and may stem from interference between multiple source mechanisms [Shera and Guinan 2003; Shera et al., 2008]. Whereas only one mechanism is represented in the current model, the gecko shows evidence for at least two different OAE generation mechanisms [Bergevin et al., 2008].

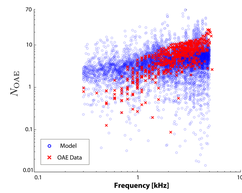

FIGURE 7 Comparison of N between model and gecko OAE data. Emission delays were measured using a 20 dB SPL probe. For the model, the only free parameter of relevance was Q, which was chosen to match observations based upon auditory nerve fiber responses at threshold.

SUMMARY

- We have described a simple model for the gecko inner ear in order to predict SFOAE magnitude and phase. When the sharpness of tuning of the model resonators is chosen to match ANF responses, the model captures many of the qualitative features of gecko SFOAEs. In particular, the model reproduces the substantial phase-gradient delays in spite of the absence of a tuned BM or traveling waves.

- The model predicts that SFOAE phase-gradient delays are proportional to the sharpness of tuning of the resonators inside the ear (i.e., hair cells and associated tectorium).

- Many mechanisms in the model are qualitatively similar to those of coherent reflection filtering [Zweig and Shera, 1995] in the mammalian cochlea (e.g., the role of a dominant spatial frequency in determining SFOAE delay).

- The oscillators used here are presumably too simple (e.g. passive, linear, no fluid coupling between adjacent bundles). Nevertheless, we conjecture that the proportionality between SFOAE delays and sharpness of tuning described here holds in more realistic models.

ANSWER: Tuned resonant elements inside the inner ear are sufficient to give rise to the long delays observed in OAEs